ADVANCED FUNCTIONAL MATERIALS
www.afm-journal.de

Materials Views
www.MaterialsViews.com

# Influence of Line Defects on the Electrical Properties of Single Crystal $TiO_2$

*Kiran Kumar Adepalli, Marion Kelsch, Rotraut Merkle,* and Joachim Maier*

**One-dimensional defects are created in [001] and [110] oriented $TiO_2$ single crystals by uniaxial pressure. Transmission electron microscopy (TEM) characterization shows them to preferably lie on {110} planes. Electrical properties studied as a function of oxygen partial pressure reveal their influence on ionic and electronic charge carriers. At high oxygen partial pressures (1 bar–$10^{-5}$ bar) the conductivity due to positive charge carriers is strongly enhanced, e.g., the ionic conductivity is increased by more than two orders of magnitude, when the electrical measurement axis lies on the slip plane. In contrary, no changes are observed when the measurement axis does not lie on the slip planes. At low oxygen partial pressures (<$10^{-15}$ bar), irrespective of orientation and presence of dislocation, there is no change in the n-type conductivity. The observed phenomena can be well explained within the space charge model, assuming the dislocation cores to exhibit an excess negative charge (increased titanium vacancy concentration). The present study gives a clear correlation between line defects and point defect concentrations in such an oxide for the first time.**

## 1. Introduction

Electrical properties of ionic solids are strongly dependent on the concentrations and mobilities of point defects. So far the main focus was laid on the fundamental understanding of bulk point defect chemistry, and modifications occurring at interfaces such as grain boundaries. In the present work we show a new approach to modify the electrical properties of ionic solids by creating 1D defects (dislocations) by mechanical action, and we can for the first time relate these changes to space charge accumulation zones around the line defects. 1D defects do not only play an intermediate thermodynamic role as far as formation is concerned, they also take an intermediate place in kinetic respects. That is the reason why electroceramic research so far concentrated on point defects (equilibrium defects) and interfaces (strongly frozen regime).

To investigate these effects in detail we chose $TiO_2$ as the model material. $TiO_2$ has become the material of interest in many fields of science. Key applications of $TiO_2$ include water splitting,[1] photocatalysis,[2] photoelectrochemical properties,[3] dye sensitized solar cells,[4] memristor and nonvolatile memory devices,[5] gas sensors,[6] and anodes for Li-batteries.[7] The variety of applications of $TiO_2$ is due to its unique chemical, optical and electrical properties. All the fore-mentioned applications and properties depend either directly or indirectly on their point defect chemistry. Therefore, the functionality of $TiO_2$ can be tuned by varying the concentrations of point and extended defects.

Up to now, the change in point defect concentrations in ionic solids is either achieved by chemical methods (doping or equilibration with different component activities, $pO_2$) or utilizing size effects.[8] The latter became of great interest recently, as it provides different properties compared to the bulk properties of the material.[9,10] Another possibility is by mechanical methods, which has not been in the focus so far. This method involves creation of extended defects such as dislocations or stacking faults in the material as result of stress applied to the lattice. Stress effects are frequently observed in epitaxial films when grown on substrates with different lattice parameter.[11,12] An easy and well known technique to generate extended defects in bulk materials involves compression experiments, where the material gets plastically deformed by slip yet without loosing the periodicity of the crystal. Numerous works[13–19,20] on $TiO_2$ focused mainly on its mechanical properties and structural deformation, but no study so far attempted to relate dislocation formation and point defect concentrations. In contrast, for halides the charged nature of dislocations and their effect on point defect concentrations (and thus electrical conductivity) was investigated more thoroughly,[21] and also a slow healing-out of these effects was observed already at room temperature.[22] For highly doped oxides such as Y-doped $ZrO_2$, introducing dislocations was found to increase the ionic conductivity by less than 10%.[23] Since the point defect concentration in such a material is already high, rather strain fields (affecting the ion mobility) are discussed for enhancing the ionic conductivity.[24] In the context of resistive switching memories, dislocations are being discussed as fast diffusion paths,[25] nevertheless for such samples which were exposed to large electrical fields in the "electroforming" step the properties of highly conductive filaments may differ from those prepared by mechanical deformation.[26]

K. K. Adepalli, Dr. R. Merkle, Prof. J. Maier
Max Planck Institute for Solid State Research
Heisenbergstrasse 1, 70569 Stuttgart, Germany
E-mail: r.merkle@fkf.mpg.de
M. Kelsch
Max Planck Institute for Intelligent Systems
Heisenbergstrasse 3, 70569 Stuttgart, Germany

DOI: 10.1002/adfm.201202256

The literature allows us to understand the nature of extended defects that are likely to be formed, which are mainly characterized by their slip systems (favorable plane and direction where defects likely form and move). Hirthe and Brittain[13,14] focused on the slip systems of rutile single crystals. In high temperature steady state creep experiments they observed that {110}<001> and {–101}<101> are the favorable slip systems. Ashbee et. al.[16] studied the stress-strain relationships for rutile single crystals as a function of crystal orientation and compression axis and found that irrespective of the orientation, the favorable slip system remained {–101}<101> and {110}<001>, with the former being more favorable than the latter at lower stresses.[17] They also extensively studied $TiO_2$ films by transmission electron microscopy (TEM) to characterize different defects.[12,15] In other studies the same slip systems were found.[19,20]

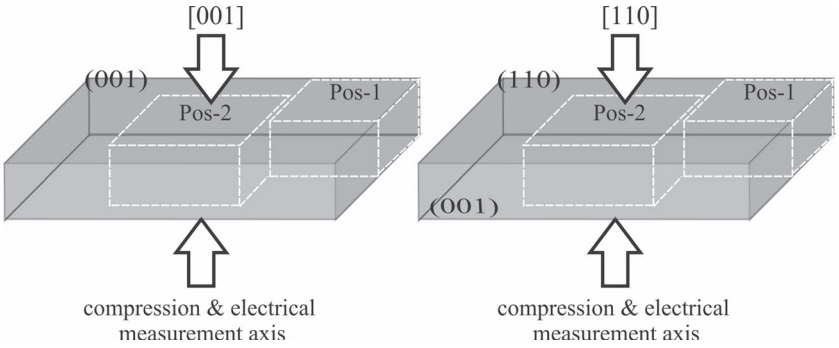


**Figure 1.** Scheme of crystal orientation with respect to the applied compressive load. Electrical measurements were performed at two locations (Pos-1 and Pos-2) by applying Pt electrodes on both sides of the large surfaces.

The electrical properties of $TiO_2$ were studied independently in the past[27–29] in slightly and strongly reducing atmosphere where nominally undoped $TiO_2$ is an n-type conductor, and in oxidizing atmosphere where rutile is p-type conducting. At intermediate temperatures, nominally undoped rutile single crystals are electronic conductors with very low ionic transference number.[27] In case of significantly doped rutile the ionic transference number depends on $pO_2$; the number is negligible at very low and high $pO_2$ and increases at intermediate $pO_2$.[29]

Based on simple mass action laws and electroneutrality conditions, the defect concentrations can be related to the oxygen partial pressure ($pO_2$) when equilibrium with gas phase is established:[28]

$$O_2 + 2\,V_O^{\cdot\cdot} \rightleftharpoons 2\,O_O^X + 4\,h^\bullet$$

The standard defect chemical treatment yields

low $pO_2$

$$2\left[V_O^{\cdot\cdot}\right] = [e'] : \sigma_{eon} \propto (pO_2)^{-1/6}$$

$$2\left[V_O^{\cdot\cdot}\right] = [A'] : \sigma_{eon} \propto (pO_2)^{-1/4}$$

intermediate $pO_2$

$$2\left[V_O^{\cdot\cdot}\right] = [A'] : \sigma_{ion} = \text{const.}$$

high $pO_2$

$$2\left[V_O^{\cdot\cdot}\right] = [A'] : \sigma_{eon} \propto (pO_2)^{1/4}$$

Therefore, a plot of conductivity versus $pO_2$ provides information about predominant carriers and charge compensation.[30] The interesting subject here will be to investigate the effect of 1D defects in single crystal $TiO_2$ on the point defects and the respective electrical properties.

Line defects (also known as 1D defects or simply dislocations) are the simplest extended defects in comparison to 2D and 3D defects in the sense of having less broken bonds involved and hence having a lower formation energy. Even though there are many ways to generate such 1D defects such as scratching the surface or polishing, uniaxial hot-pressing has the advantage to reproducibly generate a high and approximately uniform dislocation density throughout the samples. In this study, we have successfully created dislocations in [001] and [110] oriented crystals, which will be denoted as $T_{001}$ and $T_{110}$ for convenience. The choice of studying only these two orientations comes from the prior knowledge of the slip systems in $TiO_2$[12–19,20] in order to align the conductivity measurement axis either parallel or perpendicular to the slip planes. Further, the effect of slightly varying dislocation density was studied by preparing two samples from each compressed crystal; one from the corner (labeled as Pos-1) and the other from the centre (labeled as Pos-2) of the large sample as shown in **Figure 1**. We suppose that during compression there is a slight temperature gradient across the sample leading to some variation in the dislocation density. Therefore Pos-2 exhibits a higher dislocation density than the Pos-1 sample. The observed changes in the electrical properties will be discussed in terms of the space charge model.

## 2. Results and Discussion

### 2.1. TEM Characterization

**Figure 2**a shows a bright field (BF) TEM image of the $T_{001}$ sample with beam axis parallel to [001]. The dark-featured lines correspond to dislocations lying on the planes where the Bragg condition is nearly met. Translation of the reciprocal lattice vector (diffraction vector) **g** to the real space image shows that the dislocations lie on {110}. Selected area diffraction (SAD) patterns were taken at different locations on the image without tilting the sample as shown as insets in Figure 2a. Comparing the diffraction patterns reveals a small tilt in the regions above and below the array of dislocations. This can be due to the lattice strain created by the dislocations slightly bending the crystal. This array of edge dislocations can be regarded as a low angle tilt boundary. The same is also shown in high resolution JEOL 4000FX TEM (Figure 2b) covering the region with slight tilt, which is adjacent to an array of edge dislocations. **Figure 3**a shows the BF-TEM image of the sample prepared from the cross-section of $T_{100}$ with beam axis parallel to [110]. To obtain strong diffraction contrast, the sample was tilted to achieve a two beam condition with only {110} planes diffracting strongly

along with the zero beam. Figure 3b shows the dark field (DF) image of same dislocations; it is clear that the dislocations are on {110} as they appear brightly (in DF mode, the objective aperture is placed over the –110 diffraction beam to achieve specific orientation information by only illuminating the –110 planes which meet the Bragg condition). The contrast features on the top-left of the image are fringes due to thickness variation in the sample.

**Figure 4**a shows a BF-TEM image of the $T_{110}$ sample with beam axis parallel to [110]. As before, the sample was tilted to achieve a strong diffraction contrast by two beam condition with diffraction vector **g** = (001); the corresponding DF-TEM image (Figure 4b) was taken at the same place by placing the aperture over (001). To analyze the Burgers vector **b**, a dislocation has to be imaged at different diffraction vectors **g** (two beam condition); this procedure has to be repeated until the condition is found for which the dislocation vanishes ($\mathbf{g} \cdot \mathbf{b} = 0$). However, this is beyond the interest of the present study because this has been extensively characterized in the early 1960s in identifying the slip systems for rutile.[13,15,17,20] However, to compare the present results with the known slip systems from the literature, we measured the samples with two different **g** vectors operating one at a time. **Figure 5** shows such a comparison for the $T_{110}$ sample with beam parallel to [110], the operating **g** vector equals to (001) and (–110) in Figure 5a and Figure 5b respectively. Some dislocations lose the contrast when operating in **g** = (–110) condition (dislocation at position X disappears); the only possible vector that meets the $\mathbf{g} \cdot \mathbf{b} = 0$ condition with **g** being (–110) is only [001] (see ref. [15] for more explanation). With the available literature information, this short analysis is sufficient to confirm the Burgers vector to be on [001]. **Figure 6** shows a BF-TEM image of the $T_{110}$ sample obtained from the cross-section, with a two beam condition operating with **g** = (–110) and zero beam parallel to [001]. The insets show the diffraction patterns with zone parallel to [001]; there is a small tilt similar to that observed in the $T_{001}$ plan view sample (Figure 2a). At least two TEM specimens were prepared from the different locations of the sample and analyzed individually; the features remained consistent indicating dislocations formed throughout the sample. The density of dislocations as calculated from TEM images was $\approx 10^{13}$ m$^{-2}$, this corresponds to an average distance between the dislocations to be 0.3 μm (assuming pure edge type dislocations extending through the sample thickness). From Figures 2 through 6 it can be understood that the overall nature of the dislocations is the same irrespective of the compression direction (either parallel to [001] or [110]) dislocations are formed and the slip system remains unchanged, which is in well agreement with the literature.[13–19,20]

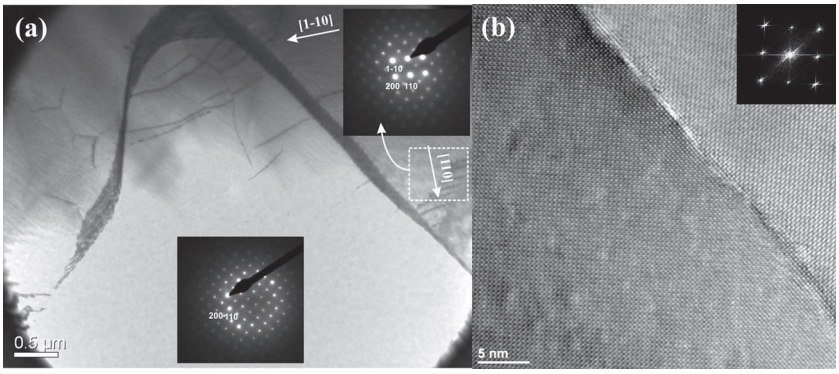


**Figure 2.** a) TEM bright field image of the $T_{001}$ sample prepared from plan view with beam axis parallel to [001]; inset shows the diffraction patterns taken at the respective locations. b) High resolution TEM image for the same sample.

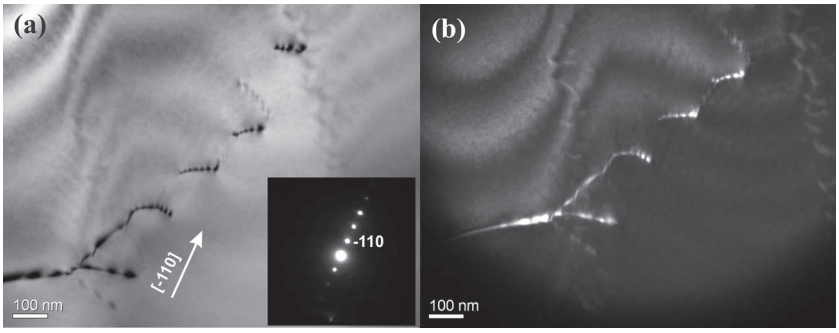


**Figure 3.** a) TEM-BF image of the $T_{001}$ sample prepared from cross-section, two beam condition with [–110] diffraction vector operating along with beam axis parallel to [110]. b) DF image with aperture over the diffraction vector [–110].

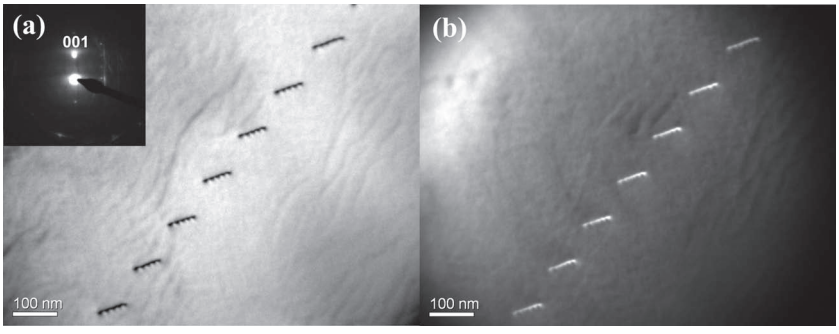


**Figure 4.** a) TEM-BF image of the $T_{110}$ plan view sample, with two beam condition operating with beam axis parallel to [110] and [001] diffraction vector. b) DF image with aperture over diffraction vector [001].

The dislocations however do not always remain a straight line (as in pure edge dislocations). As shown in the TEM images more complicated features appear by interaction with other dislocations, which is energetically favorable. Hence, a thoughtful way of characterizing the electrical properties is to measure parallel to the slip system where the measurement axis contains all

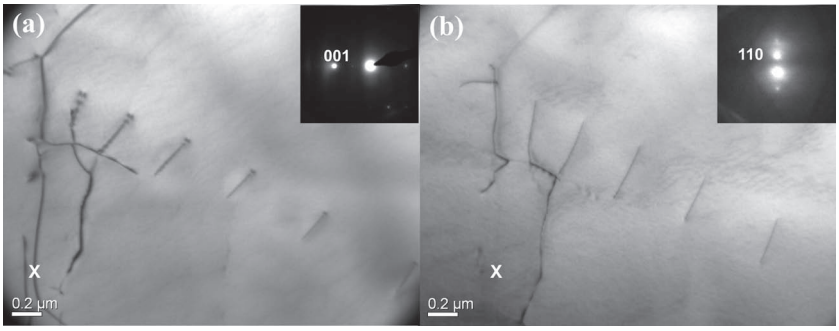


**Figure 5.** TEM-BF image of the $T_{110}$ plan view sample with beam parallel to [110]: a) two beam condition with only [001] diffraction vector and b) only [110] diffraction vector reflecting.

the planes with dislocations (as in case of $T_{001}$) and vice versa ($T_{110}$ meets this condition). This was the key motivation to choose [001] and [110] orientations in this study.

### 2.2. Electrical Characterization

In this section we will explore the effect of the dislocations on the electrical properties based on their orientation with respect to the conductivity measurement axis. The TEM characterization indicates that irrespective of the compression axis {110} are the favorable planes for the dislocations to occur. As shown in Figure 1, the conductivity measurement axis is chosen parallel to the compression axis, therefore in the $T_{001}$ sample the measuring axis lies on the slip planes of $TiO_2$ (note: dot product of their vectors is zero). However, in case of the $T_{110}$ sample, the measuring axis does not lie on the slip planes (nonzero dot product). Since the conductivity of $TiO_2$ is slightly anisotropic,[31] the $T_{001}$ and $T_{110}$ samples are plotted separately (**Figures 7** and 10) and are always compared with samples of same orientation without dislocations (labeled as pristine sample). Figure 7a shows the $pO_2$ dependence of electrical conductivity for $T_{001}$ at 823 K. The key observations are: i) at high $pO_2$ (1 bar to $10^{-5}$ bar) the overall conductivity has been strongly enhanced (higher for the sample Pos-2 with higher dislocation density) and ii) the slopes are decreased compared to the untreated crystal.

In the high-$pO_2$ regime the conductivity is due to either positive electronic defects (electron holes) or positive ionic defects (oxygen vacancies or titanium interstitials). Thus the generation of dislocations obviously also requires an increased concentration of charge-compensating negative defects. Because the acceptor impurity content did not change and the samples were properly

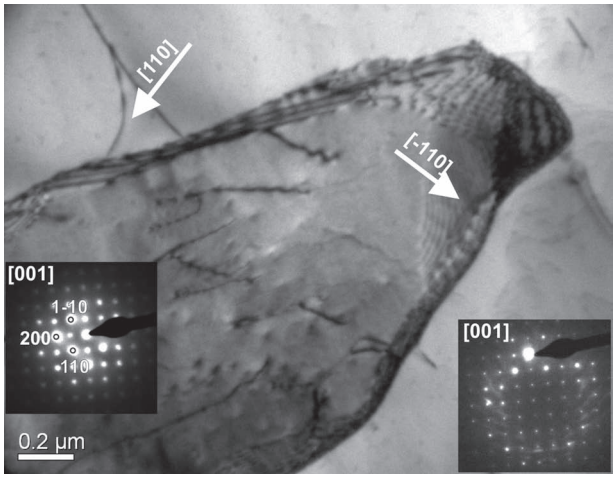


**Figure 6.** TEM-BF image of the $T_{110}$ sample prepared from cross-section, with two beam condition operating with [–110] diffraction vector and beam axis parallel to [001]. Insets show the diffraction pattern of the corresponding region.

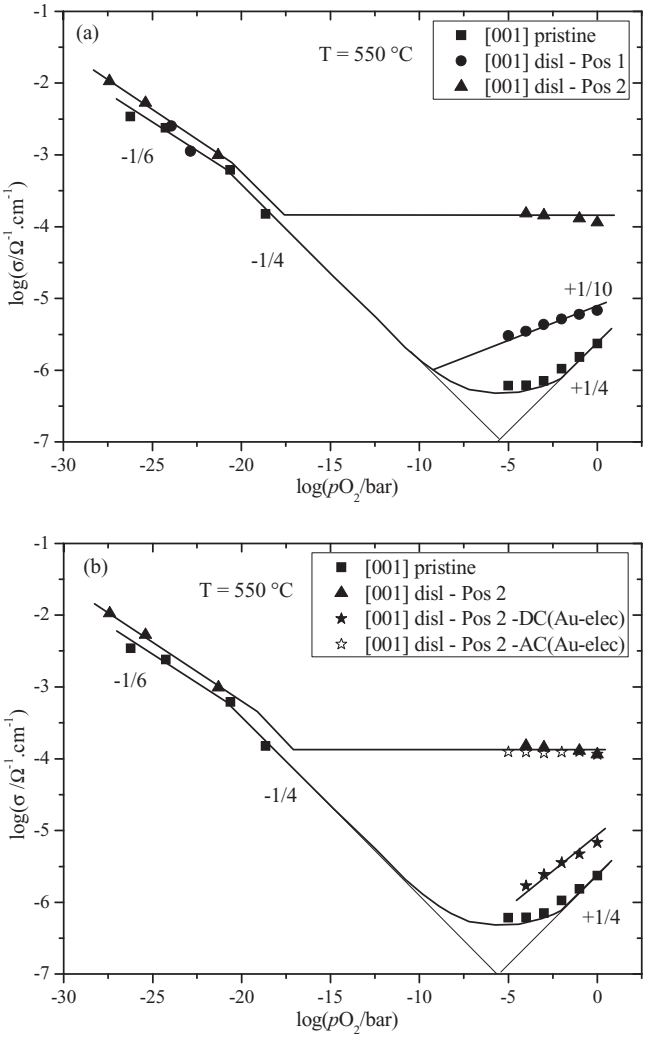


**Figure 7.** Electrical conductivity versus oxygen partial pressure measured at 823 K for the $T_{001}$ sample with conductivity measuring axis parallel to the compression axis [001] compared to a pristine sample without compression. a) AC conductivity with Pt paste electrodes and b) partial electronic conductivity of disl–Pos 2 sample by using ion blocking dense Au electrodes (represented as Au-elec). AC conductivity data of pristine and disl–Pos 2 samples are shown for comparison.

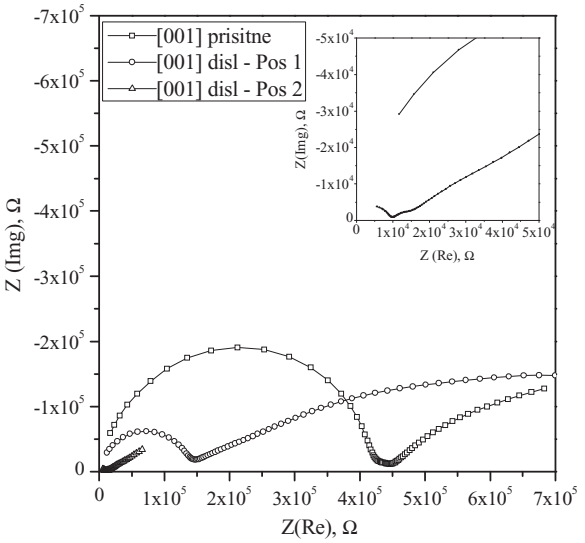


**Figure 8.** Impedance spectra of $T_{001}$ sample with and without dislocations at 823 K at 1 bar oxygen. Sample with dislocations show electrode polarization.

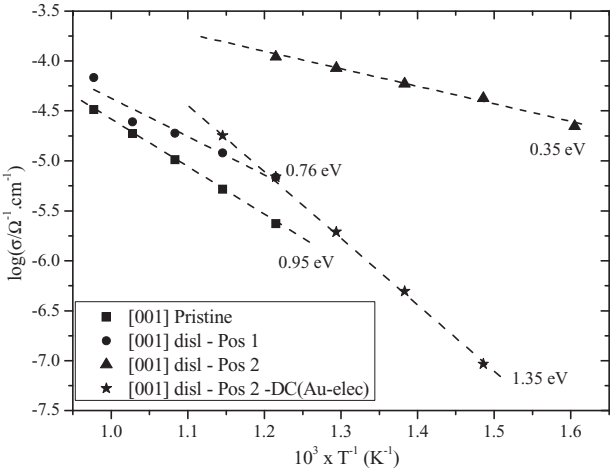


**Figure 9.** Activation enthalpy for conduction of the $T_{001}$ sample with and without dislocations measured at 1 bar oxygen.

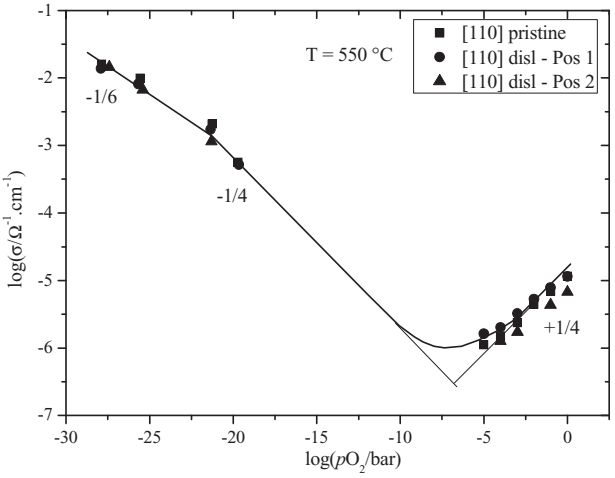


**Figure 10.** Electrical conductivity versus partial pressure of oxygen measured at 823 K for the $T_{110}$ sample with conductivity measurement axis parallel to the compression axis [110] compared to a pristine sample without compression.

re-oxidized after compression treatment, we presume that excess negative defects are formed in the dislocation cores to maintain overall electroneutrality (see Section 2.3.). In principle this could be oxygen interstitials or Ti vacancies, where the former can be regarded improbable due to the quite close-packed oxide ion lattice in rutile and the respective higher formation energies in the bulk as well as for grain boundaries.[33] DFT calculations yield a higher bulk formation energy for $O_i^{//}$ + $V_O^{\cdot\cdot}$ compared to $Ti_i^{\cdot\cdot\cdot\cdot}$ + $V_{Ti}^{////}$ (for all possible Fermi energies[32] under reducing conditions, which corresponds to the compression treatment applied here).

Hence, we suggest the creation of cation vacancies by dislocations which are immobile at the measurement conditions due to their low bulk diffusivity.[33,34] The decrease in slope can consistently be explained with an increase of the positive mobile ionic carriers in the sample (oxygen vacancies or Ti interstitials).

The impedance spectra for the samples $T_{001}$ with and without dislocations in **Figure 8** support this interpretation. The sample with dislocations shows strong electrode polarization in comparison to the pristine sample without dislocations. This is a typical phenomenon observed for blocking electrodes (at the comparably low measurement temperature ionic defects are significantly blocked at the metallic Pt electrodes). The Hebb-Wagner polarization measurement on the Pos-2 sample (with ion-blocking Au electrode) confirmed also an increase in the hole conductivity by half an order of magnitude through the presence of dislocations (see Figure 7b).[36] However the ionic contribution is far higher with an ionic transference number ranging from 0.94 to 0.99 at $pO_2$ from 1 to $10^{-5}$ bar respectively, i.e., the formation of dislocations is capable of switching the conductivity from predominant electronic to ionic.

**Figure 9** shows that the presence of the dislocations changed the activation energy for conduction in 1 bar of oxygen. This difference supports that the type of carriers changed (as concluded already from the $pO_2$ dependence). The activation energy for the sample with highest dislocation density is lower than the known ionic defect migration enthalpies[37] ($V_O^{\cdot\cdot}$ ≈ 0.8 eV and $Ti_i^{\cdot\cdot\cdot\cdot}$ ≈ 0.7 eV); this could be due to space charge accumulation effects being more pronounced at lower temperatures (see Section 2.3) and/or due to strain fields in the dislocation region facilitating ionic motion (tensile strain was found to lower ion migration barriers, e.g., in fluorite oxides).[24]

In contrast, the $T_{110}$ sample showed no change in the conductivity compared to the pristine sample without dislocations (see **Figure 10**). The slope +1/4 at high $pO_2$ (1–$10^{-5}$ bar $pO_2$) corresponds to electron hole carriers. This interpretation is also supported by the impedance spectra (**Figure 11**) where no electrode polarization is observed, pointing towards predominant electronic conductivity. The activation energy for conduction in pure oxygen is close to 1.2 eV for all [110] samples (**Figure 12**), showing no variation in conduction mechanism as well. In the

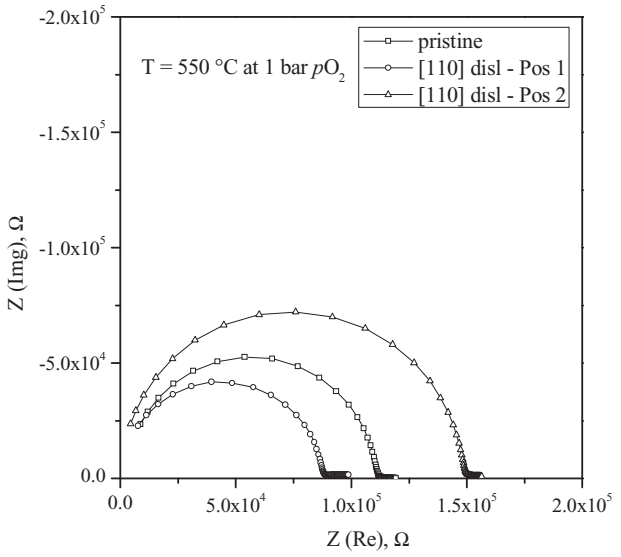


**Figure 11.** Impedance spectra of the $T_{110}$ sample with and without dislocations at 823 K at 1 bar oxygen.

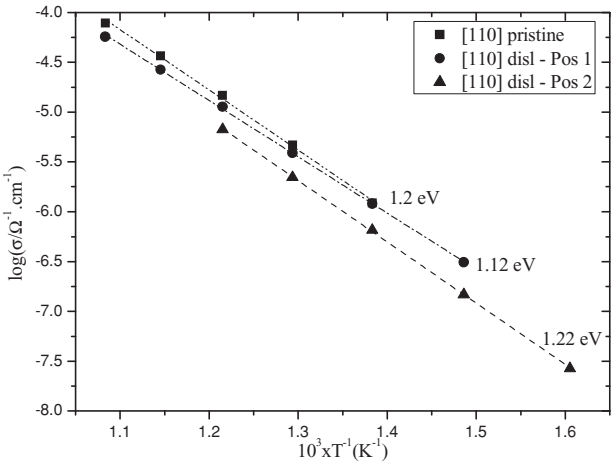


**Figure 12.** Activation enthalpy for conduction for the $T_{110}$ sample measured in 1 bar oxygen.

n-type regime ($pO_2 < 10^{-12}$ bar) there is no significant conductivity or slope change observed either in $T_{001}$ or $T_{110}$ samples after the dislocation generation.

### 2.3. Discussion

The increase in positive charge carrier concentration in the $T_{001}$ sample is only possible by presence of additional negative defects to maintain the electroneutrality condition. These negative defects are most probably Ti vacancies created in the dislocations cores. This excess negative charge formed in the dislocation cores will then be compensated by adjacent space charge layers with accumulation of mobile positive defects ($h^{\bullet}$, $V_O^{\bullet\bullet}$, $Ti_i^{\bullet\bullet\bullet\bullet}$). Such space charge zones are a common phenomenon observed at surfaces,[38] interfaces[39] and dislocations[21] for numerous ionic solids.

For many nominally undoped and acceptor-doped wide band-gap oxides, the grain boundary core exhibits an excess positive charge and adjacent space charge depletion zones;[40] this is a key reason for decreased conductivity at interfaces (blocking grain boundaries). However, in case of rutile $TiO_2$, a negative dislocation core charge and neighboring space charge accumulation layers can be regarded as the reason for the increased positive carrier conductivity as shown schematically in **Figure 13**. At high $pO_2$ in the p-type regime, when the measurement axis [001] lies on the slip planes ($T_{001}$ sample), the negative dislocation core and adjacent positive space charge accumulation layers enhance the conductivity (Gouy-Chapman situation).

In a first approximation the excess charge density in the dislocation cores can be regarded as $pO_2$-independent, i.e., we assume that charged defects are formed in the cores mainly for structural reasons (e.g., cation vacancies for avoiding otherwise too close ion contacts) and thus depend little on $pO_2$.[42] Then also the space charge potential is approximately $pO_2$-independent. The $pO_2$ dependence of defect concentrations will be the same in the space charge zone as in the bulk, and in particular the concentration of the accumulated positive majority carriers ($V_O^{\bullet\bullet}$, $Ti_i^{\bullet\bullet\bullet\bullet}$) is expected to be $pO_2$-independent, as observed in Figure 7a for the sample with high dislocation density.

The interpretation in terms of a Gouy-Chapman situation, predicting hole accumulation adjacent to the dislocations, is supported by the Hebb-Wagner polarization measurements

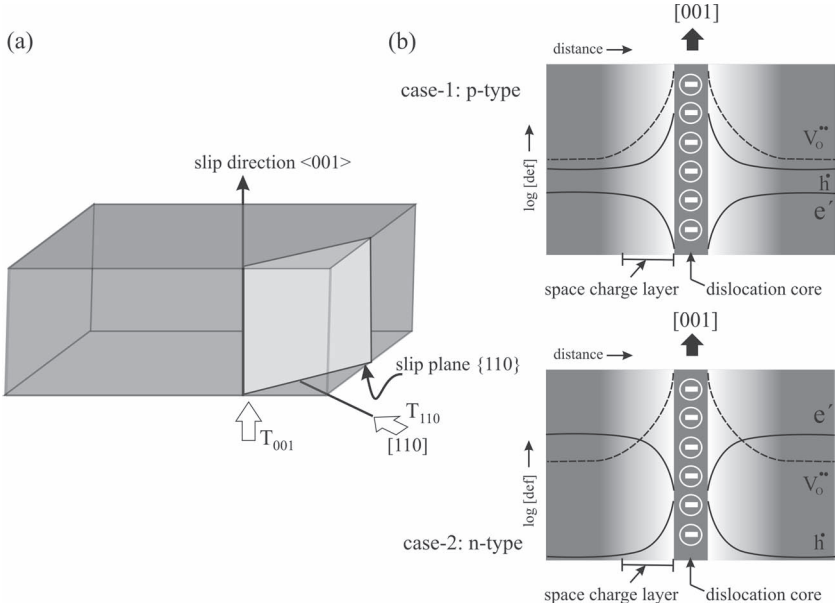


**Figure 13.** a) Schematic representation of the slip system and measurement axis (only one plane is showed for better view). b) A possible space charge model for p-type and n-type.

(Figure 7b) showing increased hole conductivity by a factor of about 5. Based on the space charge arguments (assuming unchanged defect mobilities in space charge zones) this would result in an increase by factor 25 for oxygen vacancy concentration and conductivity (due to their doubly positive charge) and 625 (≈3 orders in magnitude) for titanium interstitial conductivity. This value is very close to the observed ionic conductivity and points towards a significant contribution of titanium interstitials to the measured ionic conductivity (remember that oxygen vacancy and titanium interstitial conductivity are not distinguishable from the $pO_2$ dependence in the high $pO_2$-regime).[30] The low activation energy of the ionic conductivity (Figure 9) can arise from increased defect mobility caused by strain effects, as well as from the fact that carrier accumulation in the space charge zones becomes less pronounced at higher temperatures. Thus we cannot yet exactly quantify how much of the ionic conductivity increase might be caused by strain effects. Nevertheless, the observed enhancement of all positive charge carriers, i.e., ions as well as holes, strongly supports that space charge layer accumulation (Figure 13b case 1) is indeed the main reason for the enhanced conductivity in presence of dislocations.

The dislocation cores and space charge accumulation zones can be viewed either as a single dislocation running throughout the crystal, or as a number of shorter dislocations with space charge zones overlapping along the measurement axis to yield a percolating path with high defect concentrations. Figure 2a shows several such dislocations which are very closely spaced and also running through the entire TEM sample thickness. Regarding this as representative of the whole sample, formation of percolating pathways for enhanced conductivity appears highly probable.

However, when the measurement axis is perpendicular to the slip planes (here: $T_{110}$ sample) the influence on the conductivity is negligible (as long as the space charge zones do not overlap) as the conduction path is perpendicular to the space charge layers as shown in Figure 13a and the current essentially flows through the unmodified $TiO_2$. The condition for the space charge zone to overlap is given by $2\lambda \geq d_{dis}$ (where $\lambda$ is the Debye length and $d_{dis}$ is the distance between the dislocations), on the average this condition is not met in the $T_{110}$ samples as the calculated distance between dislocations (≈0.3 μm) is two orders of magnitude higher than the calculated Debye length[43] (≈3 nm).

This negative core charge model also explains the reason for the unchanged conductivity in the n-type regime. As shown in Figure 13b, in the n-type regime the electron concentration is higher throughout the bulk (i.e., crystal region free from dislocations and space-charge layers) and hence, conduction through the bulk lattice is preferred over the electron-depleted space-charge layers in both samples. In case of the $T_{110}$ sample, as long as the dislocation space charge zones do not form an overlapping depletion zone and do not cover a significant volume fraction (see above: extension of space charge zone is about 1% of the distance between the dislocations) these electron depletion zones do not play a significant role in the n-type regime. Hence, in the n-type regime there will be no measurable change in the electrical conductivity with respect to the measurement direction.

An alternative to the proposed model could be a model with a positive dislocation core charge (formed due to $V_O^{\cdot\cdot}$ or $Ti_i^{\cdot\cdot\cdot\cdot}$) and adjacent negative space charge zones. Even though this model could explain the conductivity enhancement in the p-type regime (if $V_O^{\cdot\cdot}$ or $Ti_i^{\cdot\cdot\cdot\cdot}$ were sufficiently mobile along the positive dislocation cores), it fails to explain the unmodified conductivity in the n-type regime. In the n-type regime it should lead to electron accumulation in the space charge zones leading to conductivity enhancement in contrast to the observations. This further supports the argument of dislocations forming a negative core by Ti vacancies.

At this point, based on $pO_2$ dependence plots we can not make any statement on the type of positive charge carrier involved in the high-$pO_2$ regime (i.e., Ti interstitials or oxygen vacancies), as both the defects gives rise to same slope $\pm 1/4$ for electronic defects and a $pO_2$-independent plateau of ionic conductivity when they compensate for the negative dislocation cores. To this end, oxygen tracer experiments are in progress to selectively probe oxygen defects.

## 3. Summary and Conclusions

The influence of extended defects on the point defect chemistry of $TiO_2$ single crystals was studied for the first time. Extended defects (1D-line defects) were created in rutile $TiO_2$ single crystals with [001] and [110] orientations. The dislocations were of the same nature irrespective of the compression axis by maintaining the same slip system. The [001] oriented sample with measurement axis parallel to the slip planes showed a strongly enhanced positive carrier conductivity due to the dislocations. In contrast, the [110] oriented sample did not show any change in conductivity despite presence of dislocations. The reasons for the increased conductivity and modified $pO_2$-dependence, caused by a change from predominant electronic to ionic conductivity, can be explained based on a negative core charge of the dislocations and adjacent space charge accumulation layers. The absence of conductivity change in the n-type regime is in line with this interpretation. This study suggests the introduction of line defects as an alternative method to tune the electrical properties of a material. As a rule of thumb, the typical temperature for the healing of line defects is approximately 0.4 times the melting point of the material; however in case of rutile it is even higher[44] (only 30% recovery after annealing for 17 h at 1000 °C). Thus the dislocations and their effect on conductivity will be persistent at intermediate temperatures. With the possibility to form dislocations by local interaction (e.g., indentation experiments), one can imagine to create spatially modified point defect concentrations (long-time persistent at moderate temperatures) which would not be possible with the usual chemical doping approach. Such a defect-chemical structuring (locally increasing both ionic and electronic carrier concentration while changing the material from predominant electronic to ionic conduction) may become relevant in fields such as information storage (where, e.g., a balanced mixed conductivity facilitates the formation of the active filaments for resistive switching) or catalysis (where not only the presence of ionic and electronic defects is important for the activity but also the spatial distribution may be decisive).

## 4. Experimental Section

*Crystal Preparation*: A $TiO_2$ single crystal boule grown in [001] direction by Verneuil-flame fusion method was purchased from Frank & Schulte GmbH. The crystal contains approx. 120 ppm of impurities as analyzed by inductively coupled plasma optical emission spectroscopy (ICP-OES), the main impurities are Al, Cr, Cu, Fe, Na and Mg. All samples were prepared from the same crystal boule with the dimensions $10 \times 10 \times 0.5$ mm$^3$ and were cut in perpendicular to [001] and [110] to obtain the large surfaces being (001) and (110) respectively. In case of the [110] oriented sample, one of the edges was cut perpendicular to [001] and vice versa.

*Dislocation Creation*: For generation of dislocations, the single crystals were held under graphite pistons with a pressure of 40 MPa at 1473 K for 5 min (HP D 5, FCT Systeme, Rauenstein, Germany). This short holding time is sufficient to generate a high density of dislocations as the temperature is sufficient ($0.7 \times$ melting temperature) to cause slip and dislocation generation in the material. The compression axis is parallel to the [001] and [110] orientation of the crystals respectively as shown in Figure 1; this also holds for electrical measurements as shown in Figure 1. The whole process was carried out under inert Ar atmosphere which together with the graphite die reduced the samples. Post-annealing was performed at 1200 °C for 5 h in air to re-oxidize the samples and to relax stresses generated in the lattice. The high density of dislocations observed in the samples after this annealing suggests that this treatment did not significantly annihilate dislocations from the samples.

*Dislocation Characterization*: For characterization of defects, at least two TEM specimens were prepared from the plan view and cross-section of the compressed sample. Specimens for TEM were prepared by the standard method[45] starting with mechanical polishing followed by dimpling and ion milling. For convenience, cross-section specimens were prepared by the tripod wedge method[45] by mechanical thinning followed by ion milling without dimpling procedure. There were no notable changes observed with either method in TEM. Characterization of dislocations was performed on a Philips CM 200 microscope with an accelerating voltage of 200 kV and a point to point resolution of 2.7 Å, equipped with a double tilt sample holder. TEM investigation of a sample without compression confirmed that sample preparation methods did not noticeably form dislocations.

*Electrical Characterization*: For the electrical characterization, two pieces of approximate size of $3 \times 3 \times 0.5$ mm$^3$ were cut from the compressed sample, one from the corner (labeled as Pos 1) and the other from the centre (labeled as Pos 2) of the large sample as shown in Figure 1. Electrodes were prepared by applying Pt paste (Heraeus, CL 11-5100; fired in air at 1000 °C for 10 min) on either side of the large surface of the samples to measure the electrical properties parallel to the compression axis which is [001] and [110]. Electrical properties were studied as a function of temperature and $pO_2$ by impedance spectroscopy (Novocontrol Alpha-A analyzer) in the frequency range 1 MHz to 1 mHz with an AC voltage of 0.1 V across the sample (test measurements with lower AC amplitude down to 1 mV did not change the shape of the spectra). The desired $pO_2$ was achieved by mixing oxygen and nitrogen for high partial pressures (1 bar to $10^{-5}$ bar) and by $CO/CO_2$ gas mixtures for low partial pressures ($\approx 10^{-16}$ to $10^{-28}$ bar) always maintaining a total flow rate of 50 mL/min. The exact $pO_2$ was determined with a custom-made lambda sensor (Pt electrodes on Yttria stabilized Zirconia tube) connected at the end of measuring cell. Prior to the actual measurement, the samples were equilibrated for one day with change in $pO_2$ or temperature. To separate the partial conductivities, an ionic blocking electrode was prepared by depositing a dense 400 nm thick layer of Au on one side of the sample. The cell configuration can be represented as - Pt/$TiO_2$ sample/Au +. For DC electrical characterization, a Keithley 236 source measure unit was used in galvanostatic mode, keeping the output voltage below 0.01 V.

## Acknowledgements

The authors would like to thank the crystal preparation group (MPI for Solid State Research, Stuttgart) for cutting the samples and A. Meyer for chemical analysis. They are grateful to Prof. Peter Van Aken, head of StEM group (MPI for Intelligent Systems, Stuttgart) for opening the TEM facility and Dr. Fritz Phillipp (MPI for Intelligent Systems, Stuttgart) for helpful discussions on TEM analysis and carefully reading the manuscript.

Received: August 9, 2012
Revised: October 3, 2012
Published online: November 7, 2012

[1] A. Fujishima, K. Honda, *Nature* **1972**, *238*, 37.
[2] O. Carp, C. L. Huisman, A. Reller, *Prog. Solid State Chem.* **2004**, *32*, 33.
[3] C. J. Barbe, F. Arendse, P. Comte, M. Jirousek, F. Lenzmann, V. Shklover, M. Gratzel, *J. Am. Ceram. Soc.* **1997**, *80*, 3157.
[4] B. O'Regan, M. Gratzel, *Nature* **1991**, *353*, 737.
[5] a) J. J. Yang, M. D. Pickett, X. Li, D. A. A. Ohlberg, D. R. Stewart, R. S. Williams, *Nat. Nanotechnol.* **2008**, *3*, 429; b) B. J. Choi, D. S. Jeong, S. K. Kim, C. Rohde, S. Choi, J. H. Oh, H. J. Kim, C. S. Hwang, K. Szot, R. Waser, B. Reichenberg, S. Tiedke, *J. Appl. Phys.* **2005**, *98*, 033715.
[6] L. D. Birkefeld, A. M. Azad, S. A. Akbar, *J. Am. Ceram. Soc.* **1992**, *75*, 2964.
[7] Y. S. Hu, L. Kienle, Y. G. Guo, J. Maier, *Adv. Mater.* **2006**, *18*, 1421.
[8] a) J. Maier, *Nat. Mater.* **2005**, *4*, 805; b) J. Maier, *Phys. Chem. Chem. Phys.* **2009**, *11*, 3011.
[9] S. Kim, J. Maier, *J. Electrochem. Soc.* **2002**, *149*, J73.
[10] P. Lupetin, G. Gregori, J. Maier, *Angew. Chem. Int. Ed.* **2010**, *49*, 10123.
[11] D. W. Pashley, *Philos. Mag.* **1959**, *4*, 324.
[12] K. H. G. Ashbee, R. E. Smallman, *Philos. Mag.* **1962**, *7*, 1933.
[13] W. M. Hirthe, J. O. Brittain, *J. Am. Ceram. Soc.* **1962**, *45*, 546.
[14] W. M. Hirthe, J. O. Brittain, *J. Am. Ceram. Soc.* **1963**, *46*, 411.
[15] K. A. G. Ashbee, R. E. Smallman, G. K. Williamson, *Proc. R. Soc. London, Ser. A* **1963**, *276*, 542.
[16] K. H. G. Ashbee, R. E. Smallman, *J. Am. Ceram. Soc.* **1963**, *46*, 211.
[17] K. H. G. Ashbee, R. E. Smallman, *Proc. R. Soc. London, Ser. A* **1963**, *274*, 195.
[18] K. H. G. Ashbee, R. E. Smallman, *Phys. Status Solidi* **1964**, *4*, 289.
[19] a) L. A. Bursill, M. G. Blanchin, *Philos. Mag. A* **1984**, *49*, 365; b) L. A. Bursill, M. G. Blanchin, A. Mebarek, D. J. Smith, *Radiat. Eff. Def. Solids* **1983**, *74*, 253; c) Y. Motohashi, M. G. Blanchin, E. Vicario, G. Fontaine, S. Otake, *Phys. Status Solidi A* **1979**, *54*, 355.
[20] M. G. Blanchin, G. Fontaine, *Phys. Status Solidi A* **1975**, *29*, 491.
[21] a) J. D. Eshelby, C. W. A. Newey, P. L. Pratt, A. B. Lidiard, *Philos. Mag.* **1958**, *3*, 75; b) R. W. Whitworth, *Adv. Phys.* **1975**, *24*, 203.
[22] J. Fleig, F. Noll, J. Maier, *Ber. Bunsen-Ges.* **1996**, *100*, 607.
[23] K. Otsuka, A. Kuwabara, A. Nakamura, T. Yamamoto, K. Matsunaga, Y. Ikuhara, *Appl. Phys. Lett.* **2003**, *82*, 877.
[24] a) C. Korte, A. Peters, J. Janek, D. Hesse, N. Zakharov, *Phys. Chem. Chem. Phys.* **2008**, *10*, 4623; b) N. Schichtel, C. Korte, D. Hesse, J. Janek, *Phys. Chem. Chem. Phys.* **2009**, *11*, 3043; c) R. A. De Souza, A. Ramadan, S. Hoerner, *Energy Environ. Sci.* **2012**, *5*, 5445; d) A. Kushima, B. Yildiz, *J. Mater. Chem.* **2010**, *20*, 4809.
[25] K. Szot, W. Speier, R. Carius, U. Zastrow, W. Beyer, *Phys. Rev. Lett.* **2002**, *88*, 075508.
[26] K. Szot, W. Speier, G. Bihlmayer, R. Waser, *Nat. Mater.* **2006**, *5*, 312.

[27] J. F. Baumard, E. Tani, *Phys. Status Solidi A* **1977**, *39*, 373.
[28] M. K. Nowotny, T. Bak, J. Nowotny, *J. Phys. Chem. B* **2006**, *110*, 16270.
[29] D. K. Lee, H. I. Yoo, *Phys. Chem. Chem. Phys.* **2008**, *10*, 6890.
[30] The same $pO_2$ exponents are obtained for $Ti_i^{\bullet\bullet\bullet\bullet}$ instead of $V_O^{\bullet\bullet}$ as dominant ionic carrier when extrinsically fixed by acceptors. However, in case of intrinsic compensation, the $pO_2$ dependency is different in other cases; if $4[Ti_i^{\bullet\bullet\bullet\bullet}] = [e']$ then $\sigma_{eon} \propto (pO_2)^{-1/5}$. Hence the slope depends on the stoichiometric window. Whether $Ti_i^{\bullet\bullet\bullet\bullet}$ or $V_O^{\bullet\bullet}$ is dominant depends on the conditions and has been a subject of debate for a long time as both the species have appreciable mobility.
[31] O. Byl, J. T. Yates Jr., *J. Phys. Chem. B* **2006**, *110*, 22966.
[32] H. Peng, *Phys. Lett. A* **2008**, *372*, 1527.
[33] B. P. Uberuaga, X. M. Bai, *J. Phys.: Condens. Mater.* **2011**, *23*, 435004.
[34] M. K. Nowotny, T. Bak, J. Nowotny, C. C. Sorrell, *Phys. Status Solidi B* **2005**, *242*, R88.
[35] J. Maier, *Ber. Bunsen-Ges.* **1989**, *93*, 1468.
[36] Since the conductivity is measured along the space charge zones and positive defects ($V_O^{\bullet\bullet}$, $Ti_i^{\bullet\bullet\bullet\bullet}$) are the majority carriers in bulk and space charge zones, the Hebb-Wagner measurements can be analyzed in the usual form, see ref. [35].
[37] a) D. K. Lee, H. I. Yoo, *Solid State Ionics* **2006**, *177*, 1; b) K. Hoshino, N. L. Peterson, C. L. Wiley, *J. Phys. Chem. Solids* **1985**, *46*, 1397.
[38] a) K. L. Kliewer, J. S. Koehler, *Phys. Rev.* **1965**, *140*, A1226; b) R. A. De Souza, M. Martin, *Phys. Chem. Chem. Phys.* **2008**, *10*, 2356.
[39] a) J. Maier, *Prog. Solid State Chem.* **1995**, *23*, 171; b) J. Jamnik, J. Maier, S. Pejovnik, *Solid State Ionics* **1995**, *75*, 51.
[40] a) X. Guo, R. Waser, *Prog. Mater. Sci.* **2006**, *51*, 151; b) I. Denk, J. Claus, J. Maier, *J. Electrochem. Soc.* **1997**, *144*, 3526; c) X. Guo, W. Sigle, J. Maier, *J. Am. Ceram. Soc.* **2003**, *86*, 77; d) M. Shirpour, R. Merkle, C. T. Lin, J. Maier, *Phys. Chem. Chem. Phys.* **2012**, *14*, 730; e) C.-T. Chen, C. E. Danel, S. Kim, *J. Mater. Chem.* **2011**, *21*, 5435; f) H. J. Park, S. Kim, *J. Phys. Chem. C* **2007**, *111*, 14903; g) A. Tschope, *Solid State Ionics* **2001**, *139*, 267.
[41] R. A. De Souza, J. Fleig, J. Maier, Z. L. Zhang, W. Sigle, M. Ruhle, *J. Appl. Phys.* **2005**, *97*, 053502.
[42] Very low $pO_2$ dependences of the space charge potential were also observed, e.g., for blocking grain boundaries in slightly Fe-doped $SrTiO_3$ bicrystals,[41] as well as for nanocrystalline $SrTiO_3$ ceramics.[10]
[43] Debye length ($\lambda$) of a material is given by the following equation $\lambda = \sqrt{\frac{\varepsilon_0 \varepsilon_r RT}{2F^2 c_d z_d^2}}$ Where $\varepsilon_r$: relative permittivity of $TiO_2$ (≈85) $c_d$: dopant concentration in mol/m$^3$ (22.2 mol/m$^3$, corresponds to the following composition of Al, Cr, Cu, Na (≈20 ppm each) and Ca, Mg, Fe, Mn (≈10 ppm each)) $z_d$: effective dopant charge (varies with dopant, for e.g., –1 for Al, –2 for Ca and –3 for Na), $F$, $\varepsilon_o$, $R$, $T$ are as usual represented in SI units. Substitution of respective values yields $\lambda \approx 3.5$ nm.
[44] H. Bell, J. T. Jones, V. Krishnam, *J. Am. Ceram. Soc.* **1972**, *55*, 6.
[45] J. Ayache, L. Beaunier, J. Boumendil, G. Ehret, D. Laub, *Sample Preparation Handbook for Transmission Electron Microscopy-Techniques*, Springer, New York **2010**.